ACS APPLIED MATERIALS & INTERFACES

www.acsami.org

Research Article

Unclogged Janus Mesh for Fog Harvesting

Joo Hee Lee, Young Jin Lee, Ho-Young Kim, Myoung-Woon Moon, and Seong Jin Kim*

Cite This: *ACS Appl. Mater. Interfaces* 2022, 14, 21713–21726

Read Online

ACCESS | Metrics & More | Article Recommendations | Supporting Information

ABSTRACT: Janus membranes with asymmetric surface wettability have been extensively utilized in various fields, including fog harvesting, because of their novel liquid transport properties. However, Janus membranes have an inherent disadvantage in terms of aerodynamic efficiency in harvesting fog because of the clogged water bridges caused by the small pore size. In the present work, we applied Janus wettability to mesh geometry with systematically varying hole sizes. For a clogged mesh with a small hole size, capillary water transport to the mesh back via the wettability gradient in the direction of fog flow helps harvest more fog by enhancing water drainage, similarly to the Janus membrane. The advantage of the capillary water transport extends to a clog-free mesh with larger hole sizes but more preferably to a Janus mesh with a superhydrophilic back, which presents the highest level of fog-harvesting yield because of the fast shedding frequency and short onset time. In contrast, a Janus mesh with a superhydrophobic front, which also has a wettability gradient along the fog flow, produces a lower fog-harvesting performance, particularly at slow fog speeds, because of the dropwise deposition of large water drops that locally disturb fog flow around a protruding water surface. On the other hand, the other type of Janus mesh with a superhydrophilic front is observed to minimize this disadvantage in the local fog flow by virtue of the filmwise deposition. It is also found that some Janus treatments can help protect mesh holes from clogging up by either forming a thin water meniscus or resisting water transport through the mesh holes.

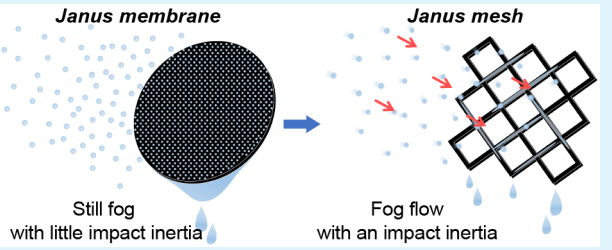

KEYWORDS: *Janus wettability, fog harvesting, filmwise deposition, dropwise deposition, clogging*

1. INTRODUCTION

Janus membranes with asymmetric surface wettability on each side have been of great interest for decades by virtue of their novel transport and selective characteristics for liquids, which can be used in a variety of filtering applications, such as oil–water separation, membrane distillation, and emulsification/demulsification.[1−3] For example, when the hydrophobic side of the Janus membrane covers an oil–water mixture, the water in contact with the membrane is spontaneously wicked toward the opposite hydrophilic side, which can be used to separate water from oil or demulsify water-in-oil emulsions.[4] Janus membranes have also been used to enhance durability in membrane distillation (MD) technology, which purifies water by collecting water vapor passed through membrane pores. Unlike traditional MD techniques that use hydrophobic membranes to block the passage of liquid water through the membrane pores, the superhydrophilic surface of the Janus membrane encloses the liquid feed solution (usually saline water or industrial water), whereas the other side of the Janus membrane with superhydrophobicity is put toward distilled water, whose state is either in the vapor or liquid phase.[5,6] Here, the superhydrophilicity helps prevent fouling of contaminants such as oil droplets and organic matter, which causes a blockage of the membrane pores by maintaining a strong adhesion between water and the membrane surface. Even if the membrane pores are partially contaminated, the outer superhydrophobic pores of the Janus membrane can still resist the passage of contaminated water to distilled water.

Recently, there have been attempts to apply the unique transport characteristics of Janus membranes to fog harvesting.[7−9] Fog indicates airborne water droplets and has recently received much industrial and environmental attention as an alternative water source.[10−12] An important industrial example is white smoke from a factory chimney.[13−16] Here, the white smoke indicates fog that forms during the evaporation of cooling water circulating inside most power plants and factories. Because of the enormous water loss in the form of white smoke (up to 27 000 L/h for a single 500 MW unit of a power plant), there is a requirement to collect the fog back to conserve industrial water.[13] Fog has also been used as drinking water in many coastal areas of Chile, Peru, and South Africa, where a fast foggy wind blows every morning from the nearby ocean.[17,18] Janus membranes are known to help improve the fog-harvesting performance by facilitating water drainage collected on the hydrophobic side because of spontaneous

Received: February 24, 2022
Accepted: April 19, 2022
Published: May 2, 2022

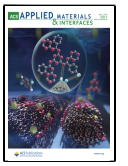

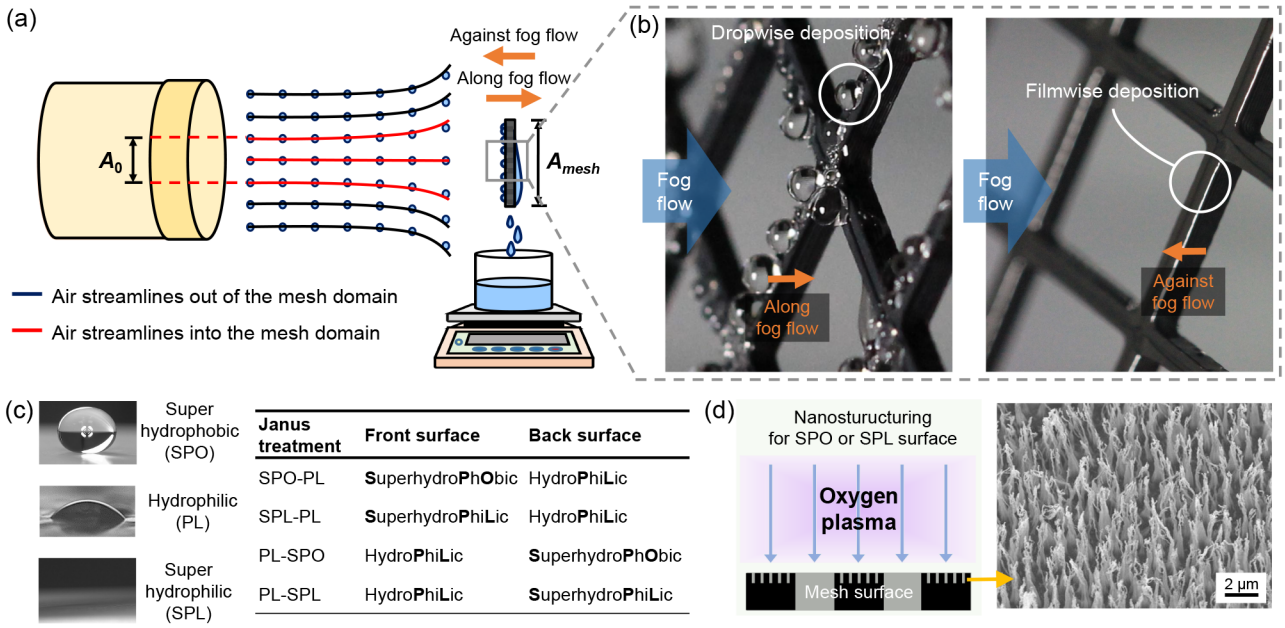

Janus treatment	Front surface	Back surface
SPO-PL	**S**uperhydro**PhO**bic	Hydro**PhiL**ic
SPL-PL	**S**uperhydro**PhiL**ic	Hydro**PhiL**ic
PL-SPO	Hydro**PhiL**ic	**S**uperhydro**PhO**bic
PL-SPL	Hydro**PhiL**ic	**S**uperhydro**PhiL**ic

Figure 1. (a) Schematic of the experimental setup to measure the fog-harvesting yield for Janus meshes with a wettability gradient either along or against the fog flow. (b) Oblique views of the examples of Janus meshes with wettability gradients along the fog flow with a superhydrophobic front (left) and against the fog flow with a superhydrophilic front (right). (c) Table of four different definitions of Janus meshes with either a superhydrophobic or superhydrophilic side on the mesh front or back. The opposite mesh surface to the superhydrophobic or superhydrophilic side has mild hydrophilicity. (d) Schematic of nanostructuring on superhydrophobic or superhydrophilic side by oxygen plasma treatment and the SEM image of the resulting nanostructure.

capillary imbibition to the opposite side with hydrophilicity.[9,19] The detailed mechanism of spontaneous capillary imbibition through a Janus membrane is described in Section S1 of the Supporting Information. The enhanced water drainage caused by this capillary imbibition also reduces the re-evaporation rate of water, which contributes to minimizing the loss of harvested water.[7,20] Because Janus membranes operate through a capillary mechanism, different Janus combinations with special wettability, such as superhydrophobic/hydrophilic or hydrophobic/superhydrophilic, have been used to help maximize the fog-harvesting performance.[8,9,21] To date, many experiments have been performed to develop an advanced Janus structure to improve fog-harvesting performance. Cao et al. suggested a composite membrane by combining two layers with contrasting wettabilities and different porosities, where a combination of a hydrophobic layer with coarser pores and a hydrophilic layer with denser pores presented high fog-harvesting performance.[7] In addition, Li et al. recently developed a three-layer sandwiched fog collector that caught fog from both sides of the fog collector by placing hydrophobic layers on the outer sides and a hydrophilic layer in the middle.[21]

Many previous studies using Janus membranes for fog harvesting mainly focused on specific environments where a foggy wind blows almost parallel to the Janus membrane, making it important to capture fog from all directions incident to the mesh.[9] However, in many situations, such as capturing white smoke from a factory chimney, it is preferable to install a fog-harvesting surface perpendicular to the fog flow to take advantage of the impact inertia of fog particles.[13,22−26] In this regard, solid meshes with subcentimeter-scaled holes have been used thus far to induce the inertial impaction of fog droplets onto the solid part of the mesh.[13,27] Although some reports have indicated that Janus membranes could be useful for increasing the fog-harvesting yield even when operating against the normal fog flow, Janus membranes are not inherently suitable for harnessing fog inertia because of their small pore size of <1 mm.[21,25,28] Because these tiny pores are subject to clogging by water bridges when harvesting fog, the Janus membrane is equivalent to an impermeable plate from an aerodynamic point of view.[29] The fog flow is then forced to detour in front of the clogged Janus membrane, which causes a significant reduction in the fog inertia toward the membrane surface. According to the well-known aerodynamic theory by Rivera, an impermeable solid plate (or a clogged membrane) has low fog-harvesting efficiency due to this detouring flow, except in a particular case where flow circumvention is limited.[29,30] As a result, a mesh with relatively large hole sizes >5 mm can avoid the adverse effects of clogging.[14,27,29]

In this paper, we applied asymmetric Janus wettability to a solid mesh with millimeter-sized holes. From the systematic variation of the mesh hole size via 3D printing, we found that the Janus effect worked differently depending on whether the mesh holes were clogged. For clogged meshes, the Janus treatment inducing capillary water transport to the mesh back, in which the mesh back has higher hydrophilicity, was found to help harvest more fog by facilitating water drainage, as similarly discussed in previous Janus membrane studies.[19,21] The advantage of capillary water transport was extended to unclogged meshes with large hole sizes. The Janus mesh with a superhydrophilic back (having a wettability gradient along the fog flow) produced the highest level of fog-harvesting yield because of the fast shedding frequency and short onset time from the enhanced water drainage. However, the Janus mesh with a superhydrophobic front, which also has a wettability gradient along the fog flow, was disadvantageous in harvesting fog, particularly at a slow fog speed, because of the dropwise deposition of large water drops that locally disturbed fog flows around a protruding water surface. On the

https://doi.org/10.1021/acsami.2c03419
ACS Appl. Mater. Interfaces 2022, 14, 21713−21726

other hand, it was found that the Janus mesh with a superhydrophilic front could minimize this disadvantage from the local fog flow disturbance and thereby maintain the high impact inertia of fog particles on the mesh strip because of the thin filmwise deposition of water on the superhydrophilic front. It was also found that some of the Janus treatments could help prevent the mesh holes from clogging up by either forming a thin water meniscus or prohibiting water passage through the mesh holes.

2. MATERIALS AND METHODS

2.1. Design of the 3D-Printed Janus Mesh. The fog-harvesting mesh was prepared using a 3D printer (CUBICON Single plus/CUBICON Inc.) to systematically control the mesh hole size of d. The hole size is a major factor in determining whether the mesh is clogged by a capillary water bridge. A mesh with a hole size much larger than the capillary length [$l_c = \sqrt{\sigma/(\rho_w g)} \approx 2.7$ mm for water] is known to be clog-free, where σ is the surface tension coefficient, ρ_w is the water density, and g is the gravitational acceleration.[29] In contrast, mesh holes with $d \ll l_c$ are entirely clogged by water bridges.[29,31] In the present work, to compare the effect of mesh clogging on fog-harvesting performance, we tested five different hole sizes of 1, 2, 5, 7, and 11 mm. Both the mesh thickness (h) and the strip width (w) were fixed to be 1 mm for all the meshes.

Janus wettability was imparted on the 3D-printed mesh by applying a plasma treatment to only one side of the mesh in an RF-CVD (radio frequency chemical vapor deposition) chamber. The as-printed poly(lactic acid) (PLA) mesh was initially hydrophobic with a static contact angle of $\theta_s = 80 \pm 1°$ that was measured by the sessile drop method, as shown in Figure 1c. A superhydrophilic surface was then provided by performing oxygen-plasma etching on the PLA surface for 40 min at a working pressure of 4 Pa and a bias voltage of −400 V. The oxygen-plasma process on the PLA surface produced a nanopillared structure,[32] as shown in the SEM (scanning electron microscopy) image of Figure 1d, and it also granted high hydrophilicity by forming multiple different groups of oxygen atoms.[33] The resulting surface had nearly zero θ_s as the water quickly wicked through the nanopillared structure. The oxygen plasma-treated surface can experience a hydrophobic recovery (aging effect), losing its hydrophilicity over time.[34] However, the current superhydrophilic surface was observed to retain its superhydrophilicity with complete wicking of zero contact angle over 5 days in both air and water as shown in Figure S2. And, because all of the fog-harvesting experiments were performed soon after the Janus mesh was prepared, the data in this paper were not affected by the aging effect.

It was observed that the bottom surface of the mesh was affected by oxygen plasma that penetrated through a nanoscale gap between the mesh bottom and the cathode in the plasma chamber as shown in Figure S3. Here, the bottom surface indicates the mesh surface in contact with the cathode during the plasma treatment. This oxygen plasma penetration was possible because the mesh strip width was as thin as 1 mm; if the mesh strip width had been wide enough, the plasma penetration would have occurred only partially at the bottom edge. As a result, mild hydrophilicity with the contact angle of 43 ± 10° was observed on the bottom surface where the nanostructure was not formed, as shown in Figure S3b. It is also worth noting that the oxygen content on the bottom surface was higher than that on the pristine PLA surface, as shown by the XPS (X-ray photoelectron spectroscopy) data in Figure S3d, which directly demonstrates the hydrophilization caused by the oxygen plasma penetration. The oxygen plasma was also observed to hydrophilize the side surface of the mesh strip to have a contact angle of 33 ± 8°, which is the value between the contact angles of the top and bottom surfaces.

A superhydrophobic surface was prepared by coating a hydrophobic nanofilm of plasma polymerized hexamethyldisiloxane (pp-HMDSO) on the superhydrophilic surface.[35] The coating process of the pp-HMDSO film was done by activating a plasma of HMDSO vapor for 30 s at a working pressure of 2.67 Pa and a bias voltage of −400 V. Then, the surface was rendered superhydrophobic with high $\theta_s = 153 \pm 2°$ following the Cassie−Baxter mechanism that describes air pockets between hydrophobic nanostructures.[36] Because of the slippery Cassie−Baxter state, the contact angle hysteresis ($= \theta_a - \theta_r$) was measured to be as small as 8 ± 2°, where θ_a is the advancing contact angle and θ_r is the receding contact angle. Unlike the oxygen plasma that penetrated beneath the mesh bottom, it was observed that the HMDSO plasma had little effect on the bottom surface presumably because of the much shorter duration of the HMDSO plasma. As a result, the bottom surface remained hydrophilic because it was already affected by the oxygen plasma penetration, but not by the HMDSO plasma. On the side surface, it was observed that the pp-HMDSO film was coated like the top surface. The XPS data in Figure Sd shows that the chemical compositions of the top and side surfaces were similar because they were coated with the same pp-HMDSO film. However, despite having a similar chemical composition, the side surface was not rendered superhydrophobic due to the lack of nanostructures with a high aspect ratio. For more information about different deposition patterns of water and chemical contents on the top, side, and bottom surfaces of superhydrophobic and superhydrophilic mesh strips, see Section S3 in the Supporting Information.

In the present work, a Janus mesh was made by applying either the superhydrophilic or superhydrophobic treatment to the mesh only once. Figure 1c tabulates four different definitions of Janus meshes of SPO-PL, SPL-PL, PL-SPO, and PL-SPL used in the present work. Here, SPO and SPL abbreviate "superhydrophobic" and "superhydrophilic", respectively. Similarly, PL stands for "hydrophilic"; please be reminded that the opposite mesh surface to the superhydrophobic or superhydrophilic surface was consistently rendered hydrophilic because of the oxygen plasma penetration. The word in front denotes wettability on the mesh's front surface, whereas the word in the back denotes wettability on the mesh's back surface: for example, SPO-PL refers to the Janus treatment with a superhydrophobic front and a hydrophilic back. Here, the front surface is the mesh surface facing the fog inlet and the back surface is opposite to the front surface, not facing the fog inlet (Figure 1a). Please do not confuse the front and back surfaces with the top and bottom surfaces. In comparison to the direction of the fog flow, Janus meshes with a more hydrophilic back (or a more hydrophobic front), such as PL-SPL and SPO-PL, have a wettability gradient along the fog flow. Janus meshes with a more hydrophilic front (or a more hydrophobic back), such as SPL-PL and PL-SPO, on the other hand, have wettability against the fog flow. Figure 1b shows examples of Janus meshes with a wettability gradient along fog flow (left) and against fog flow (right); a superhydrophobic front with dropwise deposition (left) and a superhydrophilic front with filmwise deposition (right) of the SPO-PL and SPL-PL Janus meshes are presented. The pristine PLA mesh without plasma treatment was also used in the experiment as a reference.

2.2. Fog-Harvesting Experiments. The fog-harvesting experiment was performed by shooting a fog jet from a humidifier (UH-03/JB Natural) at two different fog speeds of 0.7 and 1.3 m/s to the Janus mesh, as illustrated in Figure 1a. The average size of fog particles was measured to be 4.5 μm. More information on the measurement procedure and the size distribution of fog particles can be found in Section S4 of the Supporting Information. This fog particle size is comparable to[37,38] or slightly smaller than[39,40] values reported in previous fog-harvesting studies. The fog-harvesting experiments were conducted in an environment with a temperature of 20 ± 2 °C and a relative humidity of 80 ± 5% near the mesh. The fog inlet of the humidifier and the front surface of the mesh were placed parallel to each other. The distance between the fog inlet and the mesh was kept at 50 mm. The mesh dimensions of ∼34 mm × 34 mm was designed to be smaller than the fog inlet with a diameter of 100 mm, mimicking usual wind conditions when using fog-harvesting nets.[29] For this condition, the fog flow can circumvent out of the mesh domain, as schematically illustrated by the black streamline in Figure 1a, which can critically deteriorate the fog-harvesting performance. The fog amount, which can be captured by flowing into the mesh domain as

https://doi.org/10.1021/acsami.2c03419
ACS Appl. Mater. Interfaces 2022, 14, 21713−21726

expressed by the red streamline in Figure 1a, was previously formulated in terms of aerodynamic efficiency (η_a) by Rivera:[30]

$$\eta_a = \left(\frac{A_0}{A_{mesh}}\right)SC \quad (1)$$

where A_{mesh} is the mesh dimension and A_0 is the air flow dimension at the fog inlet, which can flow into the mesh domain, as indicated by the red streamline in comparison to the black streamline in Figure 1a. SC is called the shade coefficient, which denotes the area fraction of the solid part of the mesh surface that can capture fog particles by occluding fog flow.[29,30,38,41,42] Equation 1 states that only fog particles without significant circumvention are aerodynamically capturable. This is the reason a clogged mesh or an impermeable plate produces a low fog-harvesting yield in general,[31] except for a particular case where fog flow circumvention is limited.[29] As illustrated in Figure 1a, the water captured by the mesh was drained down to a water container on the bottom. The water weight collected in the container was then measured over time using an electronic scale (GF-603A/AND Inc.) with resolutions of 1 mg in weight and 0.5 s in time. The pressure drop across the mesh was measured using a manometer (GMH 3181-002/GHM Group).

2.3. Particle Image Velocimetry. The PIV (particle image velocimetry) experiment was performed to quantify and visualize a change in the local distortion of fog flow around a mesh strip with different deposition patterns of water. Because we are investigating the fog flow rather than the air flow, the fog particles were tracked as tracer particles. To illuminate the fog particles, we used a continuous, 10 W, 532 nm DPSS laser system (GL532T9, Shanghai Laser & Optics Century) in conjunction with a Powell lens (Thorlabs) to create the laser sheet, as schematically shown in Figure 2. The fog

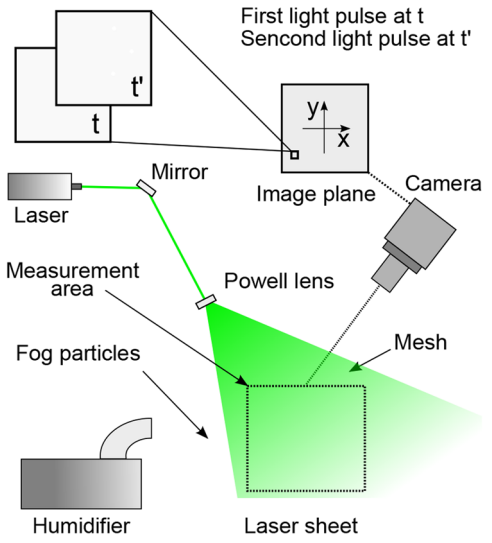

Figure 2. Schematic of the PIV experiment setup to visualize and quantify fog flow in front of a Janus mesh.

flow was recorded using a high-speed camera (FASTCAM Nova S9, Photron) with 1024 × 1024 pixel resolution at a frame rate of 6000 Hz. The recorded images were then postprocessed using PIVlab, an open-source *MATLAB*-based software,[43] to obtain the velocity field of fog flow. The image pairs were processed using the FFT window deformation algorithm to analyze the image data in several passes with a final interrogation window size of 8 × 8 pixels and 50% window overlap, resulting in a spatial resolution of 66 μm × 66 μm. Subpixel displacement was estimated using a 2 × 3 Gaussian point fit. A median filter with universal outlier detection was used to remove spurious vectors, which were subsequently replaced by interpolation. The flow fields in Figure 9c–g were then obtained by averaging the instantaneous flow fields for 500 frames, which corresponds to 83 ms at 6000 Hz.

3. RESULTS AND DISCUSSION

3.1. Janus Effect on Clogged Meshes. Figure 3 compares the fog-harvesting yield, which is the water weight collected on the bottom container after 1 h of fog-jet shooting at 0.7 m/s, for meshes with different hole sizes and different Janus treatments. Prior to discussing the Janus effect, it should be first noted that Figure 3 exhibits significantly low fog-harvesting yields for all of the 1 mm hole meshes regardless of Janus treatment in comparison to the other 5 and 7 mm hole meshes. The most notable distinction is that all of the 1 mm hole meshes were clogged by capillary water bridges, as shown in Figure 5a–e, similar to conventional Janus membranes, because of their small hole size.[29] Meshes with larger holes of 7 mm, on the contrary, were free of clogs (Figures 5p–t) because water menisci from each hole edge could not meet together to form a capillary bridge. The filled bar in the graph indicates that the mesh was completely clogged, whereas the open bar indicates that the mesh did not have a clogged hole. The half-filled bar for the untreated 5 mm hole mesh indicates that only some of the mesh holes were clogged, not all of them. As explained earlier in Section 2.2, a clogged mesh is disadvantageous for fog harvesting in terms of the aerodynamic efficiency of η_a in eq 1 because it causes significant fog-flow circumvention out of the mesh domain.[29,30] The negative effect from fog-flow circumvention can be mathematically described to decrease A_0 in eq 1, which is the fog amount that can flow into the mesh domain. In contrast, a clog-free mesh can minimize the reduction in A_0 by alleviating fog-flow circumvention.

The SPO-PL and PL-SPL Janus treatments were found to equally produce the highest fog-harvesting yield among the clogged 1 mm hole meshes. This is consistent with previous Janus membrane studies, which revealed that the Janus configuration having a wettability gradient along the fog flow (from a more hydrophobic front to a more hydrophilic back) can help enhance the fog-harvesting performance.[4] As similarly observed for previous Janus membranes,[9,21] the fogwater captured on the front of both the SPO-PL and PL-SPL meshes was transported to the mesh back following the wettability gradient and then drained from the back surface. Panels a and d in Figure 4 schematically illustrate this capillary water transport to the mesh back and subsequent drainage from the back surface by red arrows. Capillary water transport is known to help increase the fog-harvesting yield by facilitating water drainage to the bottom container.[19,21] Figure 6a plots representative temporal evolutions of the water weight collected on the bottom container, which were measured for 1 mm hole meshes with different Janus treatments. The green and purple curves for the SPO-PL and PL-SPL meshes, respectively, show more frequent increments than the other 1 mm hole meshes. This difference is more clearly presented by comparing the average shedding frequencies in Figure 7a, which demonstrates that the capillary water transport induced by either the SPO-PL or PL-SPL Janus treatment contributes to the more frequent shedding of fogwater.

It is noticeable that the other Janus meshes of SPL-PL and PL-SPO with 1 mm holes were found to harvest less fog than the untreated PLA mesh (Figure 3). This directly indicates that the Janus treatments of SPL-PL and PL-SPO had a negative effect on harvesting fog when it came to a clogged mesh. One

https://doi.org/10.1021/acsami.2c03419
ACS Appl. Mater. Interfaces 2022, 14, 21713–21726

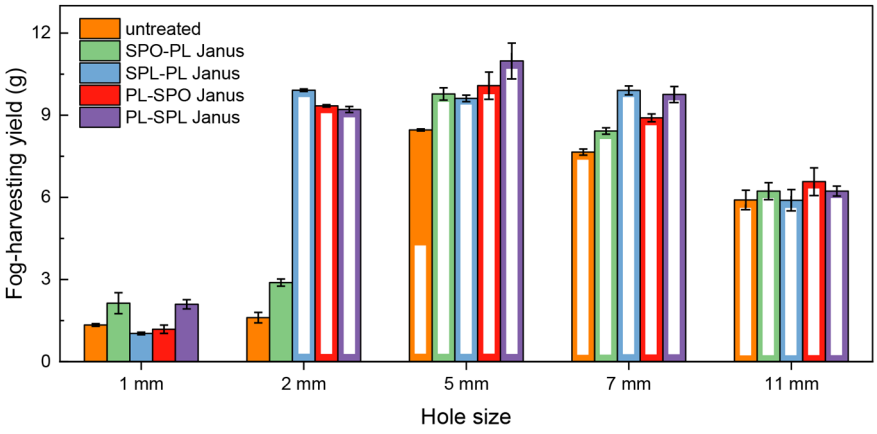

Figure 3. Bar graph of fog-harvesting yields for different types of Janus meshes with five different hole sizes. The as-printed PLA mesh without Janus treatment (untreated) was also tested as a reference. The fog-harvesting yield was measured after 1 h of fog-jet shooting at 0.7 m/s. Open bars represent meshes without a clogged hole, whereas filled and half-filled bars represent completely and partially clogged meshes, respectively.

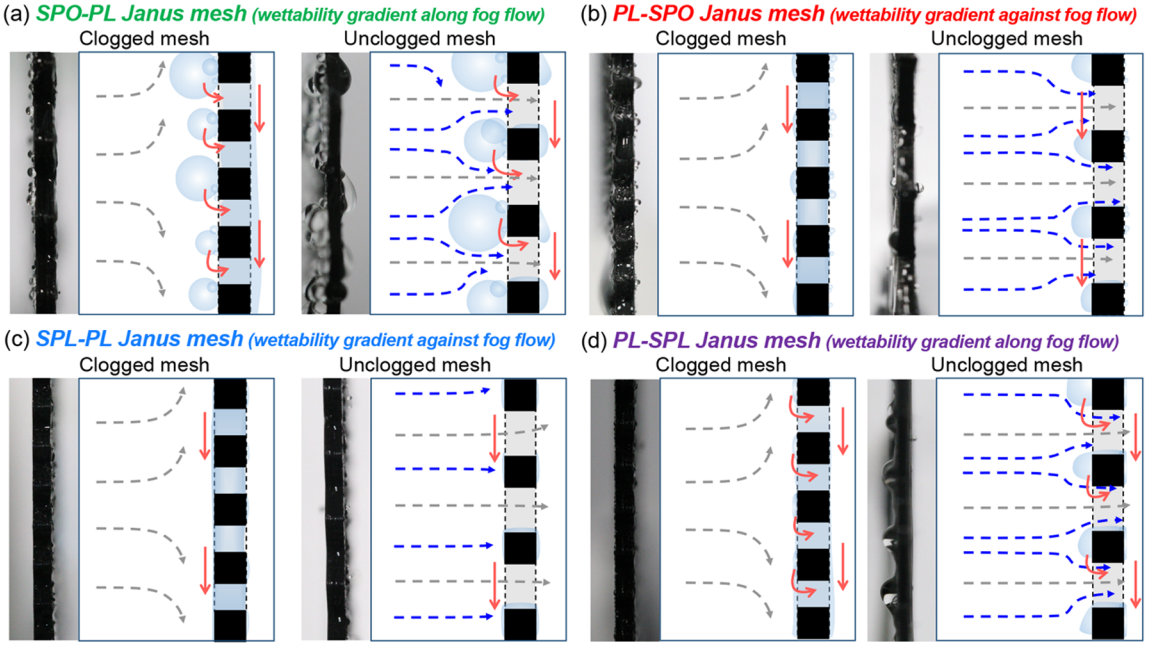

Figure 4. Experimental images and schematic illustrations of the side view of different Janus meshes with (a) a superhydrophobic front (SPO-PL), (b) a superhydrophobic back (PL-SPO), (c) a superhydrophilic front (SPL-PL), and (d) a superhydrophilic back (PL-SPL). The clogged and unclogged states of each Janus mesh are shown on each left and right, respectively.

interesting point is that these Janus meshes had a wettability gradient against the fog flow, which inhibited capillary water transport to the mesh back. Figure 7b compares the onset time, which is the time when a first water drop fell to the bottom water container. This shows that the SPL-PL mesh had the slowest onset time. This was caused by a thick water puddle on the lower edge of the SPL-PL mesh, which blocked effective drainage of water to the bottom container.[44] In addition to the slowest onset time, the SPL-PL mesh had the slowest shedding frequency (Figure 7a). The slowest onset time and shedding frequency explain why the SPL-PL mesh harvested the lowest amount of fog in the present work. Figure 8 plots the histogram of falloff drop counts with respect to the corresponding drop weight. The histogram in Figure 8d shows that the PL-SPO mesh collected relatively small water drops with a peak in the range of 60−70 mg in comparison to the untreated PLA mesh with a peak in the range of 70−80 mg (Figure 8a). Even though the SPL-PL mesh sheds relatively large water drops with the highest peak between 70−80 mg, as shown in Figure 8c, the number of shed water drops was very small because of its slowest shedding frequency and onset time.

3.2. Janus Effect on a Middle-Sized Hole Mesh ($d \approx l_c$): Clogging Criterion Reduction. Figure 3 shows that the SPO-PL mesh had the lowest fog-harvesting yield among the 2 mm hole Janus meshes. Please note that the SPO-PL mesh collected the greatest amount of fog when it came to 1 mm holes. The untreated PLA mesh was found to harvest a lower amount of fog than the 2 mm hole SPO-PL mesh. The most notable distinction from the 1 mm hole meshes is that the SPO-PL mesh and the untreated PLA mesh were clogged only among the 2 mm hole meshes, as shown in Figure 5f−j. This implies that the critical hole size that causes clogging differed between Janus treatments. The experimental image in Figure 5h shows that the 2 mm hole SPL-PL mesh with a

https://doi.org/10.1021/acsami.2c03419
ACS Appl. Mater. Interfaces 2022, 14, 21713−21726

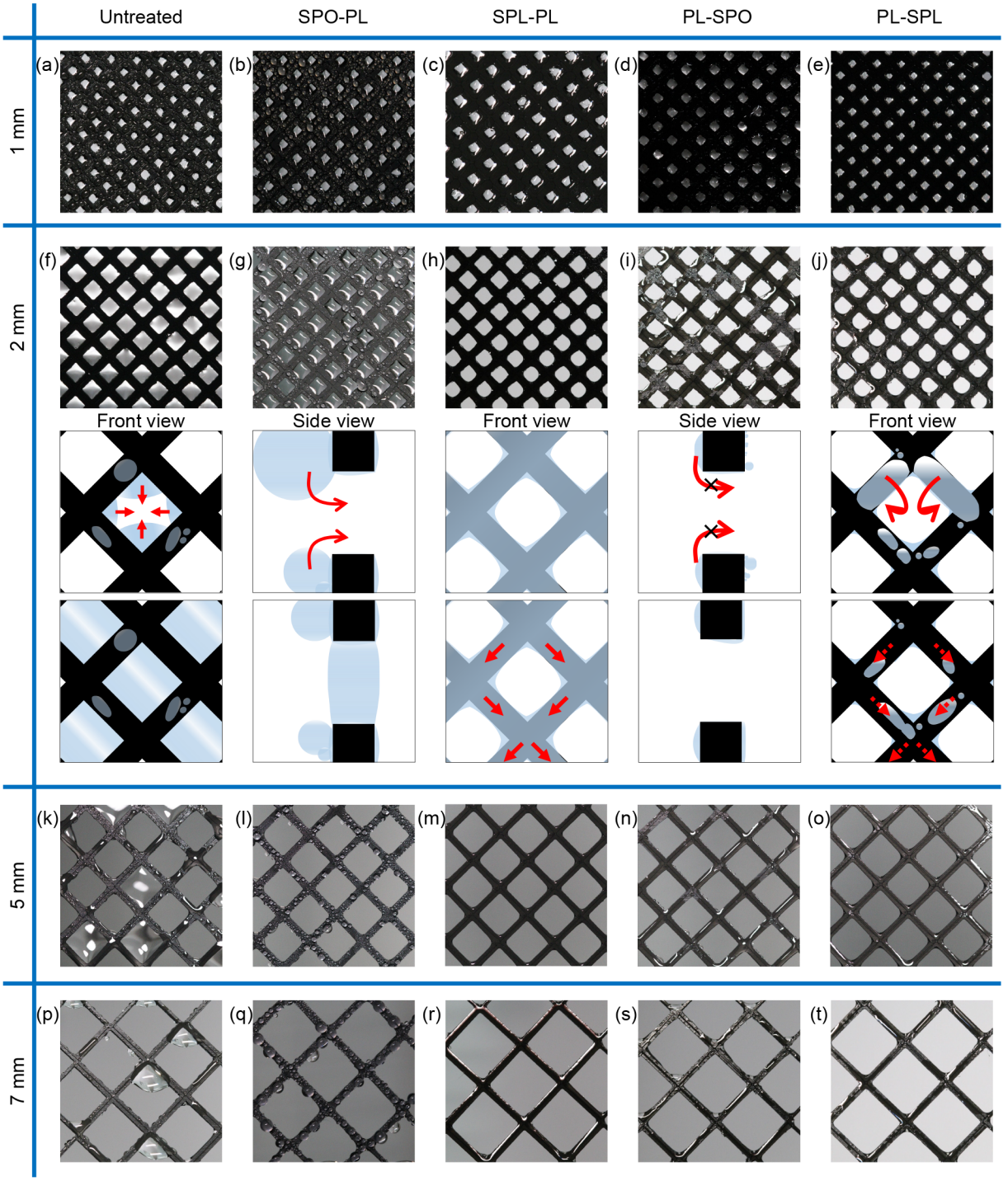

Figure 5. Front mesh surfaces with different Janus treatments and hole sizes during the fog-harvesting experiment. (a–e) All of the 1 mm hole meshes were observed to clog up regardless of the Janus treatment. (f–j) Among the 2 mm hole meshes, only the untreated mesh and the SPO-PL mesh were found to be clogged. For each case of the 2 mm hole mesh, schematic illustrations are provided to address the mechanisms that explain why some meshes were clogged, whereas others were not. (k–o) Only the untreated mesh was partially clogged among the 5 mm hole meshes. (p–t) No clogging was observed for any of the meshes with 7 mm holes, regardless of the Janus treatment.

superhydrophilic front was not clogged with more rounded hole edges formed by water menisci. This indicates that the superhydrophilicity prevents capillary clogging by suppressing the growth of the water meniscus; instead, the water keeps flowing down through the waterway along the mesh strip, as indicated by the red arrows in Figure 5h. For the 2 mm hole PL-SPO mesh, it was observed that its holes were not clogged from suppressing water passage through the mesh hole (Figure 5i). In contrast, 2 mm holes of the SPO-PL mesh became clogged by allowing water drops to travel to the mesh back, as shown in Figure 5g. The untreated PLA mesh with 2 mm holes was also found to be completely clogged, as shown in Figure 5f. Please note that the PLA mesh could neither maintain a thin water meniscus like Janus meshes with a superhydrophilic side nor block the capillary transport of water drops like the PL-SPO mesh.

https://doi.org/10.1021/acsami.2c03419
ACS Appl. Mater. Interfaces 2022, 14, 21713–21726

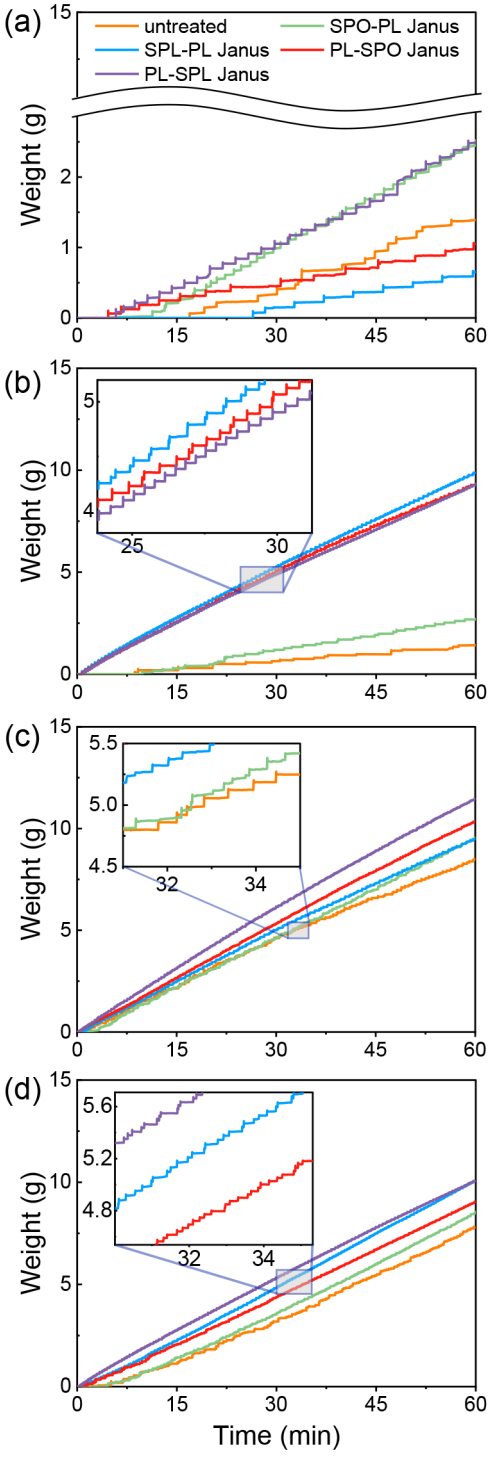

Figure 6. Representative time evolutions of water weight collected from (a) 1, (b) 2, (c) 5, and (d) 7 mm hole meshes with different Janus treatments.

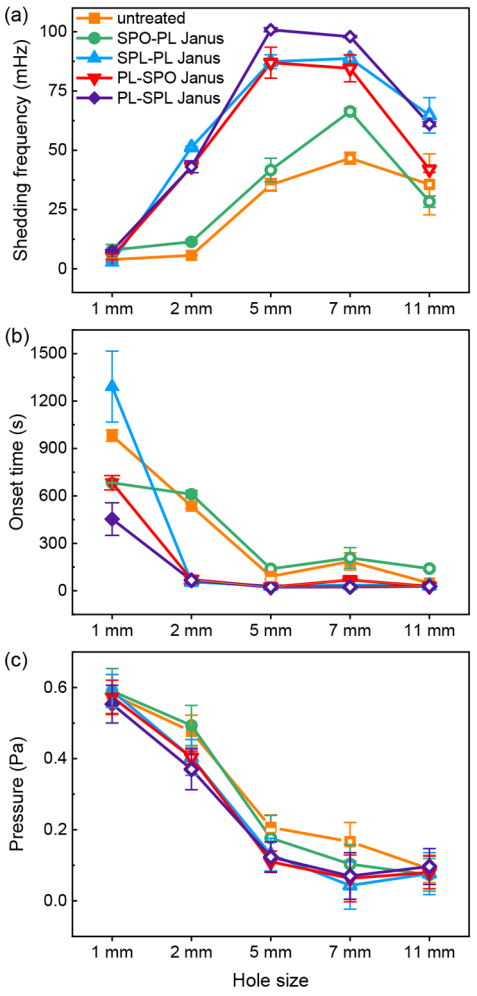

Figure 7. (a) Shedding frequency, (b) onset time, (c) and pressure drop measured for five different hole sizes of different types of Janus meshes after 1 h of fog-jet shooting at 0.7 m/s. In the plots, open symbols indicate unclogged meshes, whereas filled and half-filled symbols denote completely and partially clogged meshes, respectively.

The Janus meshes with unclogged 2 mm holes (SPL-PL, PL-SPL, and PL-SPO) were all found to have much higher fog-harvesting yields than the other clogged meshes (Figure 3) because they were free of the negative effect of fog flow circumvention from the clogged water bridges. This result again emphasizes the importance of nonclogging in fog harvesting. Figure 7a, b show that both the onset time and the shedding frequency were much faster for the unclogged 2 mm hole Janus meshes than for any other clogged meshes. The open symbols in Figure 7 denote the unclogged meshes, whereas filled and half-filled symbols represent completely and partially clogged meshes, respectively. Compared to Figure 8f–j, the drop counts from the unclogged Janus meshes were far greater than those from any other clogged meshes, which resulted from a much faster shedding frequency. Please note that the scale breaks in the *y*-axes in panels f and g in Figure 8 are given for the clogged cases because of the huge difference in the drop counts compared to the unclogged cases. The unclogged Janus meshes also had another benefit of a lower pressure drop through open holes in comparison to the clogged meshes, as shown in Figure 7c. Among the unclogged 2 mm hole Janus meshes, the SPL-PL mesh was observed to have the highest fog-harvesting yield. This is because the filmwise deposition on the superhydrophilic front minimized the aerodynamic disadvantage of the small hole size or high shade coefficient of the 2 mm hole mesh by maintaining the thinnest deposition thickness of water on the mesh surface.

Figure 8k shows that for 5 mm holes, the untreated PLA mesh was no longer completely clogged; instead, only some of the mesh holes were clogged. This partial clogging of the

https://doi.org/10.1021/acsami.2c03419
ACS Appl. Mater. Interfaces 2022, 14, 21713−21726

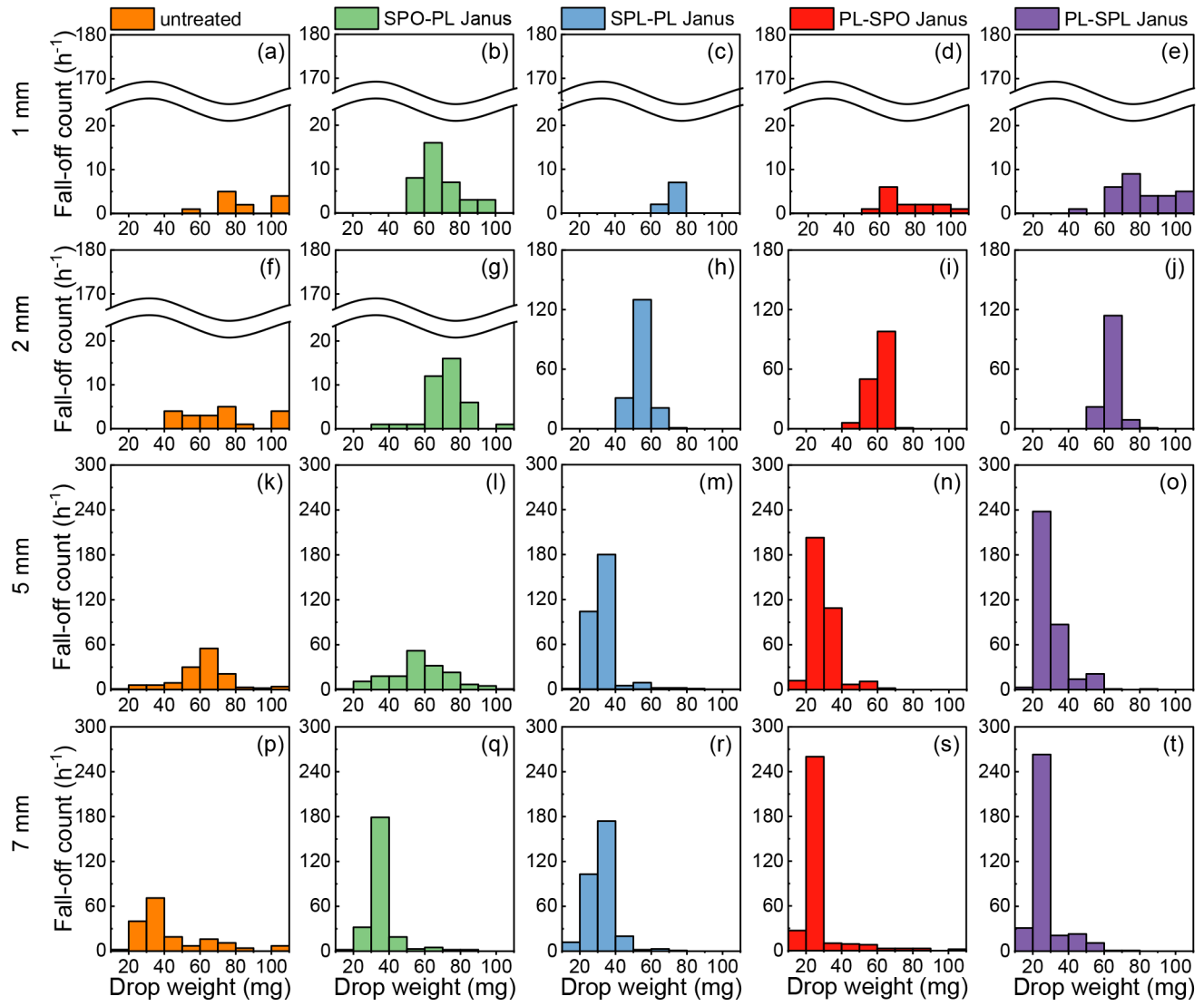

Figure 8. Histograms of the falloff count of the water drops versus their weight for (a–e) 1, (f–j) 2, (k–o) 5, and (p–t) 7 mm hole meshes with different Janus treatments. Please note that the 5 and 7 mm hole Janus meshes have much larger falloff drop counts than the other 1 mm and 2 mm hole meshes, which can be seen by the longer *y*-axis of the histograms in the bottom row.

untreated 5 mm hole mesh is known to be caused by non-self-clogging, which can occur for holes slightly larger in size than the capillary length.[29] Non-self-clogging means that the 5 mm hole cannot be clogged by merging water menisci itself. The 5 mm hole can be clogged only when there is an external water supply, such as a falling water drop, that is shed from a higher location than this hole. As the non-self-clogged water bridge is less stable because of the relatively large hole size, it may break when the water collected here drains down.[29,45] This partial clogging of the untreated 5 mm hole mesh is denoted by the half-filled bar in Figure 3. The bar graph shows that the partially clogged 5 mm hole mesh harvested much more fog than the 1 and 2 mm hole meshes with completely clogged holes because it was relatively less affected by the negative effect of clogging. However, the partially clogged PLA mesh still had a lower fog-harvesting yield than any other 5 mm hole Janus meshes without clogging. Unlike the 5 mm PLA mesh, the 5 mm hole SPO-PL mesh was observed to have no clogged holes, as shown in Figure 5l, implying that the non-self-clogging was limited on the 5 mm hole SPO-PL mesh. This is because more small water drops were transported to the mesh back and fell off the 5 mm hole SPO-PL mesh because of the low adhesion on the superhydrophobic front.

Among the unclogged 5 mm hole Janus meshes, the PL-SPL mesh presented the highest fog-harvesting yield, as plotted in Figure 3. Here, it is worth noting that the 5 mm hole PL-SPL mesh outperformed the 5 mm hole SPO-PL mesh even though they both had a wettability gradient along the fog flow and were unclogged. Please note that when their holes were completely clogged with 1 mm holes, they presented an equivalent fog-harvesting yield. Figure 5l shows that spherical water drops were deposited on the superhydrophobic front of the 5 mm hole SPO-PL mesh. The spherical curvature of the water drop contributed to a decrease in the fog-harvesting yield by allowing fog particles to pass through without being captured, which will be discussed in more detail in the next section with PIV results. The 5 mm hole PL-SPL mesh, on the other hand, had no such obstacles to local fog flow and could fully benefit from the capillary water transport by the wettability gradient along the fog flow.

https://doi.org/10.1021/acsami.2c03419
ACS Appl. Mater. Interfaces 2022, 14, 21713–21726

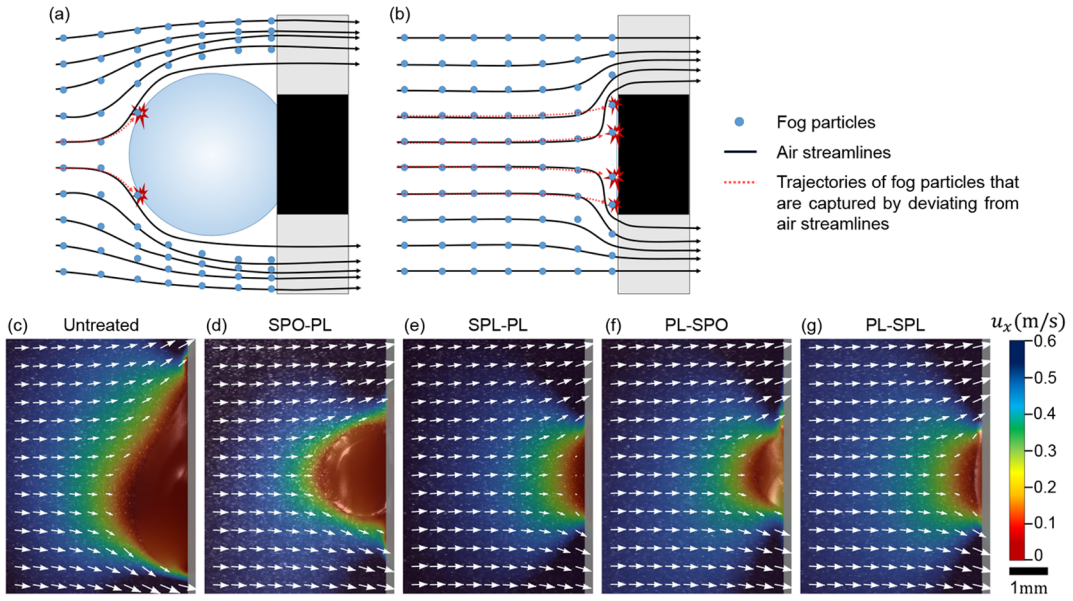

Figure 9. (a, b) Schematic illustrations presenting different particle capture behaviors around (a) a spherical water drop and (b) a mesh strip with a flat surface. (c–g) Experimentally measured velocity fields of the fog flow in front of (c) the PLA mesh and Janus meshes of (d) SPO-PL, (e) SPL-PL, (f) PL-SPO, and (g) PL-SPL with unclogged 7 mm holes, whose front surfaces have different deposition patterns of water. The color map indicates the horizontal component of fog velocity (u_x). See Movie S1 for more details.

3.3. Janus Effect on an Inherently Clogging-Free Mesh. Figure 3 shows that the fog-harvesting yield generally decreased when the hole size increased from 5 mm to 7 mm. Instead, as shown in Figure 7c, the pressure drop across the mesh was found to decrease as a trade-off for this increase in hole size. When the hole size further increased to 11 mm, however, the fog-harvesting yield drastically decreased with no compensation for the pressure drop. This implies that hole sizes larger than 11 mm will have no practical merit in both fog-harvesting yield and pressure drop. Between the 5 mm and 7 mm hole meshes, the most notable distinction was that the 5 mm hole PLA mesh was partially clogged, whereas the 7 mm hole PLA mesh was inherently clog-free when the Janus treatment was not applied. Hence, using 7 mm hole meshes, Janus effects can be discussed more apart from the influence of mesh clogging in an inherently clog-free state.

Figure 3 shows that the untreated 7 mm hole mesh collected a lower amount of fog than all of the other 7 mm hole Janus meshes. This suggests that any Janus treatment helped harvest more fog from the mesh in a clogging-free state, in contrast to the finding that only Janus treatments with a wettability gradient along the fog flow benefited the clogged mesh with 1 mm holes. Figures 5p–t compare different deposition patterns of water on the front surfaces of the 7 mm hole mesh with different Janus treatments. It was observed that huge water drops hung only on the hole edges of the untreated PLA mesh, as shown in Figure 5p. These hanging drops not only obstructed fog flow by blocking a considerable portion of the mesh hole but also allowed fog particles to pass more easily by being less captured as they flew along the curved surface of the water–air interface. Panels a and b in Figure 9 schematically depict this phenomenon by contrasting local fog flows around a curved surface of a spherical water drop (Figure 9a) and a flat surface of the mesh strip (Figure 9b). Figure 9a shows that the fog particles are less captured by better following air streamlines, denoted by black curves, that are more smoothly bent near the spherical water surface in comparison to those in Figure 9b. Here, red dotted curves represent the fog particle trajectories that can be captured by deviating from each air streamline. Please note that fog particles must deviate from the air streamlines with their higher inertia than air to be captured.[46,47] Then, as indicated by the red dotted curves, they can be captured by impacting a surface with the inertia of fog particles. Otherwise, the fog particles will pass along the air streamlines without being captured. In contrast, air streamlines are more abruptly bent in front of a flat surface of a thin mesh strip, and then fog particles deviate more easily from these highly bent air streamlines in Figure 9b. Accordingly, as indicated by the red dotted curves, more fog particles can be captured with more deviations. Figure 9c–g and Figure S1 show the results of the PIV experiment, which was performed to directly measure the velocity field of fog flow near the mesh with different Janus treatments. In the figure, the color map displays the distribution of the horizontal component of fog velocity u_x, which estimates the impact speed, or the impact inertia, of fog particles toward the mesh surface. As a background for each figure, experimental images of the side view that express different water deposition patterns on the front surface (left surface of the gray rectangle) of different meshes are presented, where the gray rectangle indicates a mesh domain. Figure 9c shows that the impact speed of fog particles was significantly reduced in front of a huge hanging drop that sagged downward because of its heavy weight. The velocity vectors in the figure indicate that the fog particles flew tangentially along the curved water surface. A noticeable point is that the range of the reduced impact speed, represented by green to red colors, reached a greater distance from the untreated PLA mesh than the other Janus meshes, as shown in Figure 9c–g. This is because the huge hanging drop blocked a considerable portion of a hole and acted as a wide wall to which fog particles approached with little inertia. This disadvantage in the fog flow is responsible for the low fog-harvesting performance of the untreated mesh, which is reflected in all aspects, such as slow shedding frequency, late

https://doi.org/10.1021/acsami.2c03419
ACS Appl. Mater. Interfaces 2022, 14, 21713–21726

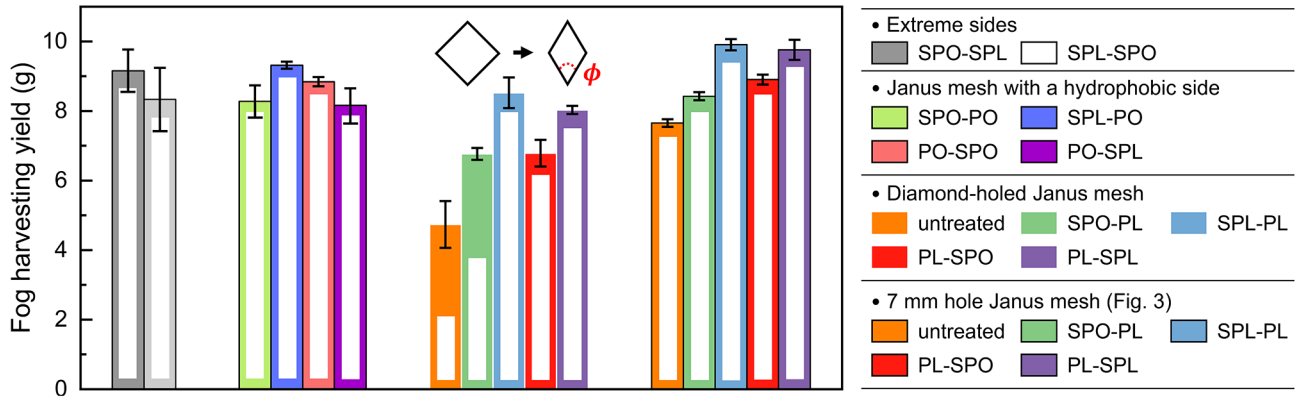

Figure 10. Comparison of the fog-harvesting yield of the Janus meshes with other wettability and geometric configurations. Except for the diamond-holed meshes, all of the meshes had 7 mm holes. Open bars represent meshes without a clogged hole, whereas half-filled bars represent partially clogged meshes.

onset time, higher pressure drop, and small drop size, as shown in Figures 7 and 8p.

On the superhydrophobic front of the 7 mm hole SPO-PL mesh, the dropwise deposition of large water drops in a spherical shape, whose diameter was larger than the mesh strip width, was observed, as shown in Figure 5q. These spherical water drops caused local distortion of fog flow around the protruding circular water−air interface in a similar way that the hanging drops did but to a lesser extent because its size was smaller than the hanging drop. Figure 9d and Movie S1 show that the impact speed of fog particles was precedently decelerated near the circular surface of a large water drop. The velocity field in the figure shows that the fog particles detoured locally around the circular water drop and flowed out through the mesh hole, resulting in less capture. Similar numerical results were previously reported in which particulate matter was captured less by a circular geometry than a square geometry because the circular geometry was more disadvantageous for intercepting particles than the square geometry.[48−50] Because of this disadvantage in the local fog flow, the SPO-PL mesh had a low fog-harvesting yield despite the benefit from capillary water transport.

The PL-SPL mesh, which is another type of mesh that can induce capillary water transport to the mesh back, is less susceptible to the negative effects of dropwise deposition. Figure 5t shows that water drops on the PL-SPL mesh front were kept thin due to the superhydrophilicity on the mesh back, which pulled back the water drops when their size increased to reach the mesh strip edge. From this capillary imbibition, the water drop on the front PLA surface of PL-SPL mesh could maintain its thin thickness (Figure 9g); please note that its drop thickness was thinner than that on the front surface of the PL-SPO mesh which obstructed water transport to the mesh back (Figure 9f). According to the fog flow field in Figure 9g, the PL-SPL mesh can suffer less from the negative effect of the dropwise deposition, unlike the SPO-PL mesh, and then fully benefit from the capillary water transport, resulting in high fog-harvesting performance. Figure 9e and Movie S1 show that the fog particles could impact more straightly toward the flat front of the SPL-PL mesh owing to the filmwise deposition. This fog particle behavior is similar to that depicted in Figure 9b, which describes the most favorable geometry configuration, in terms of aerodynamics, for capturing fog particles. The 7 mm hole SPL-PL mesh could harvest a large amount of fog because of this aerodynamic advantage.

3.4. Other Configurations in Janus Mesh and Fog Speed Variation. In addition to the four Janus configurations discussed until the last section, additional wettability and geometric configurations were investigated to provide more information on the design of Janus mesh. The fog-harvesting yields from these Janus meshes are plotted in Figure 10, where the experiment was performed at a fog speed of 0.7 m/s. Please note that all of the meshes in Figure 10 had the 7 mm holes except for the diamond-holed meshes that will be discussed later. And, on the far right side of the graph, the results from the 7 mm hole Janus meshes of SPO-PL, SPL-PL, PL-SPO, and PL-SPL (the same data as in Figure 3) were plotted again to help better comparison of the fog-harvesting yield.

The SPO-SPL mesh was prepared by plasma treating both sides of the mesh to have a superhydrophobic front and a superhydrophilic back, and the SPL-SPO mesh is the opposite case. These SPO-SPL and SPL-SPO meshes were tested to check whether a higher wettability contrast between the two sides increases fog-harvesting yield via enhanced water transport. Figure 10 shows that the SPO-SPL mesh harvested more fog than the SPO-PL mesh, indicating that the increased wettability gradient along the fog flow, which was caused by having a superhydrophilic back, contributed to the higher fog-harvesting yield. It was observed that the water drops deposited on the superhydrophobic front of the SPO-SPL mesh were transported more quickly to the superhydrophilic back than those deposited on the SPO-PL mesh. However, because of the aerodynamic disadvantage from the dropwise deposition of large spherical water drops on the superhydrophobic front, it still produced a low fog-harvesting yield in comparison to the SPL-PL and PL-SPL meshes. The SPL-SPO mesh, on the other hand, showed no significant improvement in the fog-harvesting yield when compared to the PL-SPO mesh. This is because the increased wettability gradient against the fog flow slowed the water drainage by resisting water transport to the mesh back, and the SPL-SPO mesh did not receive the same aerodynamic benefits as the SPL-PL mesh that had the thinnest water meniscus.

Figure 10 also presents the fog-harvesting yield from the Janus meshes with a hydrophobic side (SPO-PO, SPL-PO, PO-SPO, and PO-SPL), rather than a hydrophilic side. These Janus meshes were prepared by coating the opposite side of the superhydrophobic or superhydrophilic surface with a hydro-

https://doi.org/10.1021/acsami.2c03419
ACS Appl. Mater. Interfaces 2022, 14, 21713−21726

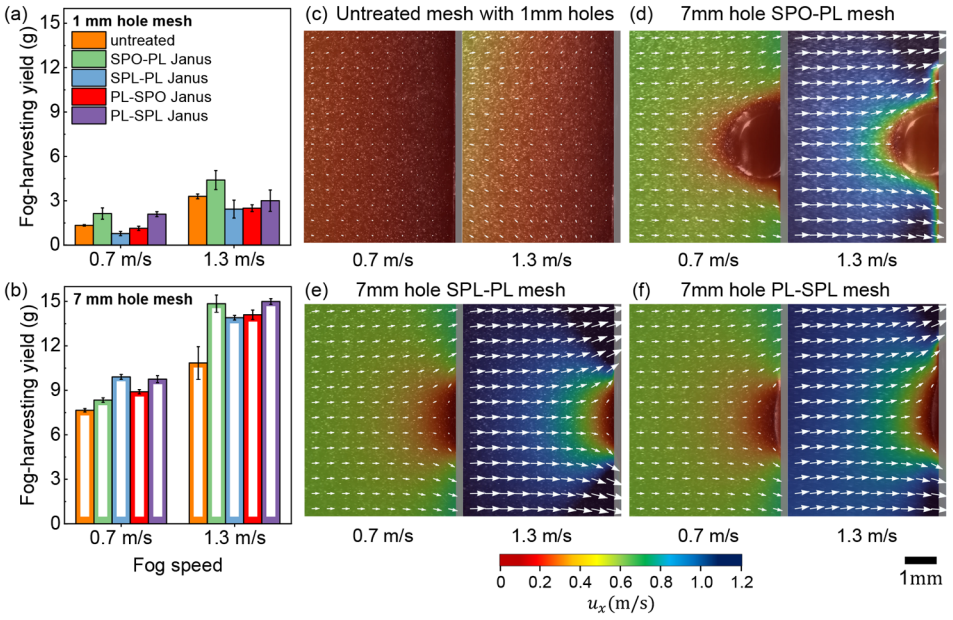

Figure 11. Comparison of the fog-harvesting yields between two different fog speeds of 0.7 and 1.3 m/s for (a) clogged meshes with 1 mm holes and (b) clog-free meshes with 7 mm holes. In the plots, filled bars represent a completely clogged mesh, whereas open bars represent meshes without a clogged hole. (c–f) Different changes in the velocity field of the fog flow in front of different types of meshes with an increase in the fog speed from 0.7 to 1.3 m/s.

phobic nanofilm, whose contact angle is 103 ± 4°, using the HMDSO plasma. The fog-harvesting yields from these Janus meshes with a hydrophobic side exhibited similar patterns to those of the Janus meshes with a hydrophilic side. This is because water transport in the Janus mesh was primarily driven by extreme wettability of superhydrophobicity (slippery Cassie–Baxter state) and superhydrophilicity (complete wicking), rather than mild hydrophobicity or mild hydrophilicity. However, the PO-SPL mesh was notably observed to have a lower fog-harvesting yield than the PL-SPL mesh because the water drops deposited on the hydrophobic front of the PO-SPL mesh disrupted the fog flow until their contact line reached the mesh strip edge and they were transported to the mesh back. In contrast, the hydrophilic front of the PL-SPL mesh had a less protruding water drop and thus was less affected by this negative effect.

The fog-harvesting yield from the diamond-holed Janus meshes is also presented in Figure 10. Here, the diamond-holed mesh was designed by distorting the geometry of the 7 mm hole mesh with square holes to have diamond holes with ϕ = 45° for the diamond-holed mesh to have the same shade coefficient as the 7 mm hole mesh, where ϕ is the angle at the hole bottom as shown in the schematic of Figure 10. The diamond-holed Janus meshes were investigated to see if there is a synergy effect between mesh geometry and Janus wettability for optimal water drainage to improve the fog-harvesting yield further. According to previous study,[51] the diamond hole with ϕ = 45° can help facilitate water drainage along the mesh strip surface. The Janus treatments of SPO-PL, SPL-PL, PL-SPO, and PL-SPL were then applied to the diamond-holed mesh geometry. Figure S6a shows that the non-self-clogging was observed on the diamond-holed SPO-PL mesh; please note that it was clog-free before being distorted to the diamond shape. Because of this non-self-clogging, the untreated diamond-hole mesh had a significantly lower fog-harvesting yield than the other unclogged meshes (Figure 10). In addition to the untreated diamond-holed mesh, the SPO-PL diamond-holed mesh was observed to have a non-self-clogged hole on a rare occasion. Apart from the untreated and SPO-PL cases, all of the other diamond-holed Janus meshes were observed to be clog-free, which indicates that the discussion on the clogging criterion reduction by the Janus treatments of SPL-PL, PL-SPO, and PL-SPL still holds. However, even though these diamond-holed Janus meshes were unclogged, their fog-harvesting yields were generally lower than those of the square-holed Janus meshes (Figure 10). This implies that the negative effect from the narrowed hole size in the horizontal direction acted more significantly to deteriorate the fog-harvesting yield, outweighing any potential positive effect from the diamond hole. However, it is not desirable to jump to conclusions based on this result that the diamond-holed Janus mesh will always produce worse fog-harvesting performance than the square-holed Janus mesh. To reach a more comprehensive conclusion, future work is required to systematically control the angle of ϕ, as well as the horizontal and vertical hole sizes and investigate their effects on fog-harvesting performance.

We then remark that the response to faster fog speeds differs between the clogged and clog-free meshes. Panels a and b in Figure 11 compare the fog-harvesting yields between (a) the clogged 1 mm hole and (b) the clog-free 7 mm hole meshes for a faster fog speed of 1.3 m/s in comparison to 0.7 m/s. Even though the fog-harvesting yield generally increased for all the meshes with a faster fog speed,[52] the bar graphs show a relatively minor enhancement in the fog-harvesting yield for the clogged meshes (Figure 11a) in comparison to the clog-free meshes (Figure 11b). This is because, despite the increase in the fog speed, the flow resistance from the clogged wall suppressed the enhancement in the impact inertia of nearby fog particles.[29] The velocity fields in Figure 11c demonstrate that there was only a minor enhancement in the impact inertia of fog particles in front of the clogged mesh with 1 mm holes

https://doi.org/10.1021/acsami.2c03419
ACS Appl. Mater. Interfaces 2022, 14, 21713–21726

despite the increase in the fog speed. In contrast, the 7 mm hole Janus meshes showed a more noticeable enhancement in the fog inertia for the faster fog speed, as shown in Figure 11d–f. This again emphasizes that the clogging-free mesh is superior to the clogged mesh for harnessing fog inertia to capture the fog particles. It is worth noting that the Janus meshes with a wettability gradient along the fog flow presented more enhancement in the fog-harvesting yield, for the faster fog speed than the other types of Janus meshes having a wettability gradient against the fog flow. This is because the faster air flow could help transport water more quickly as the air flow and wettability gradient both acted in the same direction to push water to the mesh back. One observation in Figure 11b is that the fog-harvesting yield from the 7 mm hole SPO-PL mesh improved significantly under the faster fog speed, even though it still allowed the large water drops on the front surface, as shown in Figure 11d. The difference observed during the fog-harvesting experiment for the SPO-PL mesh was that the water on the front surface was transported to the mesh back more quickly with the faster fog speed; the large spherical water drops stayed on the superhydrophobic front for a shorter period of time, which alleviated the negative effect of the dropwise deposition in the fog harvesting.

Finally, we compare the fog-harvesting yield observed in this paper to those reported in other recent previous works within last three years that used clogged Janus meshes and membranes. Here, the previous works in Table 1 were selected as those that obtained fog-harvesting yield in a similar experimental condition to ours, by hanging a Janus mesh vertically to capture fog particles whose flow direction is normal to the mesh surface. The two best records of the fog-harvesting yield for two different cases as unclogged and clogged Janus meshes were listed as the data in the present work. It is worth noting that most of the previous records of fog-harvesting yield were in the same order ~0.1 g/(cm^2 h) as the value from the clogged Janus mesh in this work. This is understandable given that the clogged Janus mesh in this work was investigated to mimic the conventional Janus membrane and compare its fog-harvesting performance to that of unclogged Janus mesh. And, as discussed earlier, the unclogged Janus mesh was found to present a superior fog-harvesting yield compared to the other recent previous values from clogged Janus meshes and membranes because the unclogged holes helped minimize the negative aerodynamic effect that reduces the impact inertia of fog particles.

Table 1. Comparison of the Fog-Harvesting Yield in This Work to Those from Recent Previous Works That Used Janus Treatments[a]

materials	best record of fog-harvesting yield (g/cm^2 h)
unclogged Janus mesh (present work)	1.30
clogged Janus mesh (present work)	0.38
sandwiched Janus net[21]	0.37
Janus fiber mesh[19]	0.07
Janus wood membrane[20]	0.29
Janus copper foam[53]	0.22
Janus porous membrane[54]	0.50
hybrid Janus mesh[55]	0.57

[a]Please note that except for the unclogged Janus mesh in the present work, all of the specimens were subject to clogging because of small pore or hole sizes.

4. CONCLUSION

In the present work, we applied asymmetric Janus wettability to the mesh geometry with a systematic change in the mesh hole size. For a hole size small enough in comparison to the capillary length, where all of the mesh holes are clogged, Janus treatments with a wettability gradient along the fog flow (more hydrophilicity on the mesh back such as PL-SPL and SPO-PL) are found to help harvest more fog by facilitating water drainage due to capillary water transport to the mesh back, as similarly discussed in previous studies on Janus membranes that are also clogged by small pore sizes. In contrast, a wettability gradient against the fog flow (more hydrophilicity on the mesh front such as SPL-PL and PL-SPO) is observed to deteriorate the fog-harvesting performance of the clogged mesh, which is even worse than that of the PLA mesh without the Janus treatment. The advantage of the capillary water transport to the mesh back is found to extend to unclogged meshes with larger hole sizes. However, when comparing two unclogged Janus meshes with a wettability gradient along the fog flow, the SPO-PL mesh harvests a lower amount of fog than the PL-SPL mesh, particularly at slow fog speeds <1 m/s, because of the deposition pattern of large spherical water drops on its superhydrophobic front. These water drops, whose sizes are larger than the mesh strip width, are observed to reduce the impact inertia of fog particles by locally disturbing the fog flow near the protruding water surface, resulting in lower fog-harvesting performance. The PL-SPL mesh does not have such large water drops because capillary imbibition from the superhydrophilic back continuously transports water to the mesh back. By virtue of capillary water transport, the PL-SPL mesh with unclogged holes can produce the highest level of fog-harvesting yield with a fast shedding frequency and short onset time. Meanwhile, it is also found that the superhydrophilic front of the SPL-PL mesh can contribute to fog harvesting by providing an aerodynamically most favorable environment for fog particles to impact more straight on toward its flat surface with filmwise deposition. Furthermore, some Janus treatments can protect mesh holes with hole sizes similar to the capillary length from clogging up by either forming a thin water meniscus (SPL-PL and PL-SPL) or resisting water transport through the mesh holes (PL-SPO).

■ ASSOCIATED CONTENT

Supporting Information

The Supporting Information is available free of charge at https://pubs.acs.org/doi/10.1021/acsami.2c03419.

Water transport mechanism, hydrophobic recovery, different surfaces of the superhydrophobic and superhydrophilic mesh strips, fog particle size measurement, fog-harvesting yield versus different types of Janus treatments (PDF)

Movie S1, results of PIV experiment (MP4)

■ AUTHOR INFORMATION

Corresponding Author

Seong Jin Kim − *Extreme Materials Research Center, Korea Institute of Science and Technology, Seoul 02792, Korea;* orcid.org/0000-0002-9405-2375; Email: kyk756@kist.re.kr

https://doi.org/10.1021/acsami.2c03419
ACS Appl. Mater. Interfaces 2022, 14, 21713−21726

Authors

Joo Hee Lee − *Extreme Materials Research Center, Korea Institute of Science and Technology, Seoul 02792, Korea*

Young Jin Lee − *Extreme Materials Research Center, Korea Institute of Science and Technology, Seoul 02792, Korea;* orcid.org/0000-0002-1396-7355

Ho-Young Kim − *Department of Mechanical Engineering, Seoul National University, Seoul 08826, Korea*

Myoung-Woon Moon − *Extreme Materials Research Center, Korea Institute of Science and Technology, Seoul 02792, Korea;* orcid.org/0000-0003-1560-1565

Complete contact information is available at: https://pubs.acs.org/10.1021/acsami.2c03419

Notes

The authors declare no competing financial interest.

■ ACKNOWLEDGMENTS

This work was supported by a KIST internal project (2E31751) and grants funded by the Korea Coast Guard (KIMST-20210584) and the Korea Ministry of Environment (MOE, 2021002800005). H.Y.K. acknowledges support from the National Research Foundation of Korea (NRF, 2018-052541). S.J.K. thanks the National Research Foundation of Korea (2020M3E9A1113568) for support and Kyuhyong Kim for assistance on the PIV experiments.

■ REFERENCES

(1) Yang, H.-C.; Hou, J.; Chen, V.; Xu, Z.-K. Janus membranes: exploring duality for advanced separation. *Angew. Chem.* **2016**, *55*, 13398−13407.

(2) Afsari, M.; Shon, H. K.; Tijing, L. D. Janus membranes for membrane distillation: Recent advances and challenges. *Adv. Colloid Interface Sci.* **2021**, *289*, 102362.

(3) Yang, H.-C.; Xie, Y.; Hou, J.; Cheetham, A. K.; Chen, V.; Darling, S. B. Janus membranes: creating asymmetry for energy efficiency. *Adv. Mater.* **2018**, *30*, 1801495.

(4) Zhou, H.; Guo, Z. Superwetting Janus membranes: focusing on unidirectional transport behaviors and multiple applications. *J. Mater. Chem. A.* **2019**, *7*, 12921−12950.

(5) Li, M.; Lu, K. J.; Wang, L.; Zhang, X.; Chung, T.-S. Janus membranes with asymmetric wettability via a layer-by-layer coating strategy for robust membrane distillation. *J. Membr. Sci.* **2020**, *603*, 118031.

(6) Huang, Y.-X.; Wang, Z.; Jin, J.; Lin, S. Novel Janus membrane for membrane distillation with simultaneous fouling and wetting resistance. *Environ. Sci. Technol.* **2017**, *51*, 13304−13310.

(7) Cao, M.; Xiao, J.; Yu, C.; Li, K.; Jiang, L. Hydrophobic/hydrophilic cooperative Janus system for enhancement of fog collection. *Small* **2015**, *11*, 4379−4384.

(8) Ren, F.; Li, G.; Zhang, Z.; Zhang, X.; Fan, H.; Zhou, C.; Wang, Y.; Zhang, Y.; Wang, C.; Mu, K.; et al. A single-layer Janus membrane with dual gradient conical micropore arrays for self-driving fog collection. *J. Mater. Chem. A* **2017**, *5*, 18403−18408.

(9) Yin, K.; Yang, S.; Dong, X.; Chu, D.; Duan, J.-A.; He, J. Ultrafast achievement of a superhydrofphilic/hydrophobic janus foam by femtosecond laser ablation for directional water transport and efficient fog harvesting. *ACS Appl. Mater. Interfaces* **2018**, *10*, 31433−31440.

(10) Korkmaz, S.; Kariper, İ. A. Fog harvesting against water shortage. *Environ. Chem. Lett.* **2020**, *18*, 361−375.

(11) Kaseke, K. F.; Wang, L. Fog and dew as potable water resources: Maximizing harvesting potential and water quality concerns. *GeoHealth* **2018**, *2*, 327−332.

(12) Yu, Z.; Zhang, H.; Huang, J.; Li, S.; Zhang, S.; Cheng, Y.; Mao, J.; Dong, X.; Gao, S.; Wang, S.; et al. Namib desert beetle inspired special patterned fabric with programmable and gradient wettability for efficient fog harvesting. *Journal of Materials Science & Technology* **2021**, *61*, 85−92.

(13) Ghosh, R.; Ray, T. K.; Ganguly, R. Cooling tower fog harvesting in power plants-A pilot study. *Energy* **2015**, *89*, 1018−1028.

(14) Ghosh, R.; Ganguly, R. Fog harvesting from cooling towers using metal mesh: Effects of aerodynamic, deposition, and drainage efficiencies. *Proc. Inst. Mech. Eng., Part A* **2020**, *234*, 994.

(15) Ghosh, R.; Ganguly, R. *Droplet and Spray Transport: Paradigms and Applications*; Springer, 2018; pp 237−266.

(16) Veldhuizen, H.; Ledbetter, J. Cooling tower fog: control and abatement. *J. Air Pollut. Control Assoc.* **1971**, *21*, 21−24.

(17) Klemm, O.; Schemenauer, R. S.; Lummerich, A.; Cereceda, P.; Marzol, V.; Corell, D.; Van Heerden, J.; Reinhard, D.; Gherezghiher, T.; Olivier, J.; et al. Fog as a fresh-water resource: overview and perspectives. *Ambio* **2012**, *41*, 221−234.

(18) Schemenauer, R. S.; Cereceda, P. Fog collection's role in water planning for developing countries. *Nat. Resour. Forum* **1994**, *18*, 91−100.

(19) Knapczyk-Korczak, J.; Zhu, J.; Ura, D. P.; Szewczyk, P. K.; Gruszczyński, A.; Benker, L.; Agarwal, S.; Stachewicz, U. Enhanced Water Harvesting System and Mechanical Performance from Janus Fibers with Polystyrene and Cellulose Acetate. *ACS Sustainable Chem. Eng.* **2021**, *9*, 180−188.

(20) Ding, Y.; Tu, K.; Burgert, I.; Keplinger, T. Janus wood membranes for autonomous water transport and fog collection. *J. Mater. Chem. A* **2020**, *8*, 22001−22008.

(21) Li, J.; Li, W.; Han, X.; Wang, L. Sandwiched nets for efficient direction-independent fog collection. *J. Colloid Interface Sci.* **2021**, *581*, 545−551.

(22) Yin, K.; Du, H.; Dong, X.; Wang, C.; Duan, J.-A.; He, J. A simple way to achieve bioinspired hybrid wettability surface with micro/nanopatterns for efficient fog collection. *Nanoscale* **2017**, *9*, 14620−14626.

(23) Carvajal, D.; Silva-Llanca, L.; Larraguibel, D.; González, B. On the aerodynamic fog collection efficiency of fog water collectors via three-dimensional numerical simulations. *Atmos. Res.* **2020**, *245*, 105123.

(24) Bai, H.; Zhang, C.; Long, Z.; Geng, H.; Ba, T.; Fan, Y.; Yu, C.; Li, K.; Cao, M.; Jiang, L. A hierarchical hydrophilic/hydrophobic cooperative fog collector possessing self-pumped droplet delivering ability. *Journal of Materials Chemistry A* **2018**, *6*, 20966−20972.

(25) Song, Y.-y.; Liu, Y.; Jiang, H.-b.; Li, S.-y.; Kaya, C.; Stegmaier, T.; Han, Z.-w.; Ren, L.-q. A bioinspired structured graphene surface with tunable wetting and high wearable properties for efficient fog collection. *Nanoscale* **2018**, *10*, 16127−16137.

(26) Su, Y.; Chen, L.; Jiao, Y.; Zhang, J.; Li, C.; Zhang, Y.; Zhang, Y. Hierarchical Hydrophilic/Hydrophobic/Bumpy Janus Membrane Fabricated by Femtosecond Laser Ablation for Highly Efficient Fog Harvesting. *ACS Appl. Mater. Interfaces* **2021**, *13*, 26542−26550.

(27) Ghosh, R.; Patra, C.; Singh, P.; Ganguly, R.; Sahu, R. P.; Zhitomirsky, I.; Puri, I. K. Influence of metal mesh wettability on fog harvesting in industrial cooling towers. *Appl. Therm. Eng.* **2020**, *181*, 115963.

(28) Zhong, L.; Feng, J.; Guo, Z. An alternating nanoscale (hydrophilic-hydrophobic)/hydrophilic Janus cooperative copper mesh fabricated by a simple liquidus modification for efficient fog harvesting. *J. Mater. Chem. A* **2019**, *7*, 8405−8413.

(29) Park, J.; Lee, C.; Lee, S.; Cho, H.; Moon, M.-W.; Kim, S. J. Clogged water bridges for fog harvesting. *Soft Matter* **2021**, *17*, 136−144.

(30) de Dios Rivera, J. Aerodynamic collection efficiency of fog water collectors. *Atmos. Res.* **2011**, *102*, 335−342.

(31) Shi, W.; Anderson, M. J.; Tulkoff, J. B.; Kennedy, B. S.; Boreyko, J. B. Fog harvesting with harps. *ACS Appl. Mater. Interfaces* **2018**, *10*, 11979−11986.

(32) Ko, T.-J.; Park, S. J.; Kim, M.-S.; Yoon, S. M.; Kim, S. J.; Oh, K. H.; Nahm, S.; Moon, M.-W. Single-step plasma-induced hierarchical structures for tunable water adhesion. *Sci. Rep.* **2020**, *10*, 1−11.

(33) Izdebska-Podsiadły, J.; Dörsam, E. Storage stability of the oxygen plasma-modified PLA film. *Bull. Mater. Sci.* **2021**, *44*, 1−9.
(34) Ren, Y.; Xu, L.; Wang, C.; Wang, X.; Ding, Z.; Chen, Y. Effect of dielectric barrier discharge treatment on surface nanostructure and wettability of polylactic acid (PLA) nonwoven fabrics. *Appl. Surf. Sci.* **2017**, *426*, 612−621.
(35) Kim, S. J.; Song, E.; Jo, K.; Yun, T.; Moon, M.-W.; Lee, K.-R. Composite oxygen-barrier coating on a polypropylene food container. *Thin solid films* **2013**, *540*, 112−117.
(36) Cassie, A.; Baxter, S. Wettability of porous surfaces. *Trans. Faraday Soc.* **1944**, *40*, 546−551.
(37) Ji, K.; Zhang, J.; Chen, J.; Meng, G.; Ding, Y.; Dai, Z. Centrifugation-assisted fog-collecting abilities of metal-foam structures with different surface wettabilities. *ACS Appl. Mater. Interfaces* **2016**, *8*, 10005−10013.
(38) Park, K.-C.; Chhatre, S. S.; Srinivasan, S.; Cohen, R. E.; McKinley, G. H. Optimal Design of Permeable Fiber Network Structures for Fog Harvesting. *Langmuir* **2013**, *29*, 13269−13277.
(39) Li, J.; Ran, R.; Wang, H.; Wang, Y.; Chen, Y.; Niu, S.; Arratia, P. E.; Yang, S. Aerodynamics-assisted, efficient and scalable kirigami fog collectors. *Nat. Commun.* **2021**, *12*, 1−8.
(40) Jiang, Y.; Machado, C.; Savarirayan, S.; Patankar, N. A.; Park, K.-C. Onset time of fog collection. *Soft Matter* **2019**, *15*, 6779−6783.
(41) Regalado, C. M.; Ritter, A. The design of an optimal fog water collector: A theoretical analysis. *Atmos. Res.* **2016**, *178*, 45−54.
(42) Yu, Z.; Li, S.; Liu, M.; Zhu, R.; Yu, M.; Dong, X.; Sun, Y.; Fu, S. A dual-biomimetic knitted fabric with a manipulable structure and wettability for highly efficient fog harvesting. *Journal of Materials Chemistry A* **2021**, *10*, 304−312.
(43) Thielicke, W.; Stamhuis, E. PIVlab−towards user-friendly, affordable and accurate digital particle image velocimetry in MATLAB. *J. Open Res. Software* **2014**, *2*, e30.
(44) Lee, A.; Moon, M.-W.; Lim, H.; Kim, W.-D.; Kim, H.-Y. Water harvest via dewing. *Langmuir* **2012**, *28*, 10183−10191.
(45) Meseguer, J.; Slobozhanin, L.; Perales, J. A review on the stability of liquid bridges. *Adv. Space Res.* **1995**, *16*, 5−14.
(46) Miguel, A. F. *Industrial and Technological Applications of Transport in Porous Materials*; Springer, 2013; pp 63−90.
(47) Mead-Hunter, R.; King, A. J.; Mullins, B. J. Aerosol-mist coalescing filters−A review. *Sep. Purif. Technol.* **2014**, *133*, 484−506.
(48) Fan, J.; Lominé, F.; Hellou, M. Numerical Investigation of the Influence of Fiber Geometry on Filtration Performance With a Coupled Lattice Boltzmann−Discrete Element Method. *J. Appl. Mech.* **2020**, *87*, 011005.
(49) Wang, K.; Zhao, H. The influence of fiber geometry and orientation angle on filtration performance. *Aerosol Sci. Technol.* **2015**, *49*, 75−85.
(50) Yu, Z.; Zhu, T.; Zhang, J.; Ge, M.; Fu, S.; Lai, Y. Fog Harvesting Devices Inspired from Single to Multiple Creatures: Current Progress and Future Perspective. *Adv. Funct. Mater.* **2022**, 2200359.
(51) von Spreckelsen, R. M.; Harris, M. T.; Wigzell, J. M.; Fraser, R. C.; Carletto, A.; Mosquin, D. P.; Justice, D.; Badyal, J. P. S. Bioinspired breathable architecture for water harvesting. *Sci. Rep.* **2015**, *5*, 1−6.
(52) Bai, H.; Zhao, T.; Wang, X.; Wu, Y.; Li, K.; Yu, C.; Jiang, L.; Cao, M. Cactus kirigami for efficient fog harvesting: simplifying a 3D cactus into 2D paper art. *Journal of Materials Chemistry A* **2020**, *8*, 13452−13458.
(53) Zhou, H.; Jing, X.; Guo, Z. Excellent fog droplets collector via an extremely stable hybrid hydrophobic-hydrophilic surface and Janus copper foam integrative system with hierarchical micro/nanostructures. *J. Colloid Interface Sci.* **2020**, *561*, 730−740.
(54) Wang, Z.; Song, S.; Yang, J.; Liu, X.; Sherazi, T. A.; Li, S.; Zhang, S. Controllable Janus porous membrane with liquids manipulation for diverse intelligent energy-free applications. *J. Membr. Sci.* **2020**, *601*, 117954.
(55) Gou, X.; Guo, Z. Hybrid Hydrophilic-Hydrophobic CuO@TiO2-Coated Copper Mesh for Efficient Water Harvesting. *Langmuir* **2020**, *36*, 64−73.

https://doi.org/10.1021/acsami.2c03419
ACS Appl. Mater. Interfaces 2022, 14, 21713−21726